Electrodeposited $NiFe_2Se_4$ on nickel foam as binder-free electrode for high performance asymmetric supercapacitor

Beirong Ye, Xianjun Cao, Qiang Zhao*, Jinshu Wang

School of Materials and Energy, University of Electronic Science and Technology of China, Chengdu 610054, China

* Corresponding author: zqphys@uestc.edu.cn

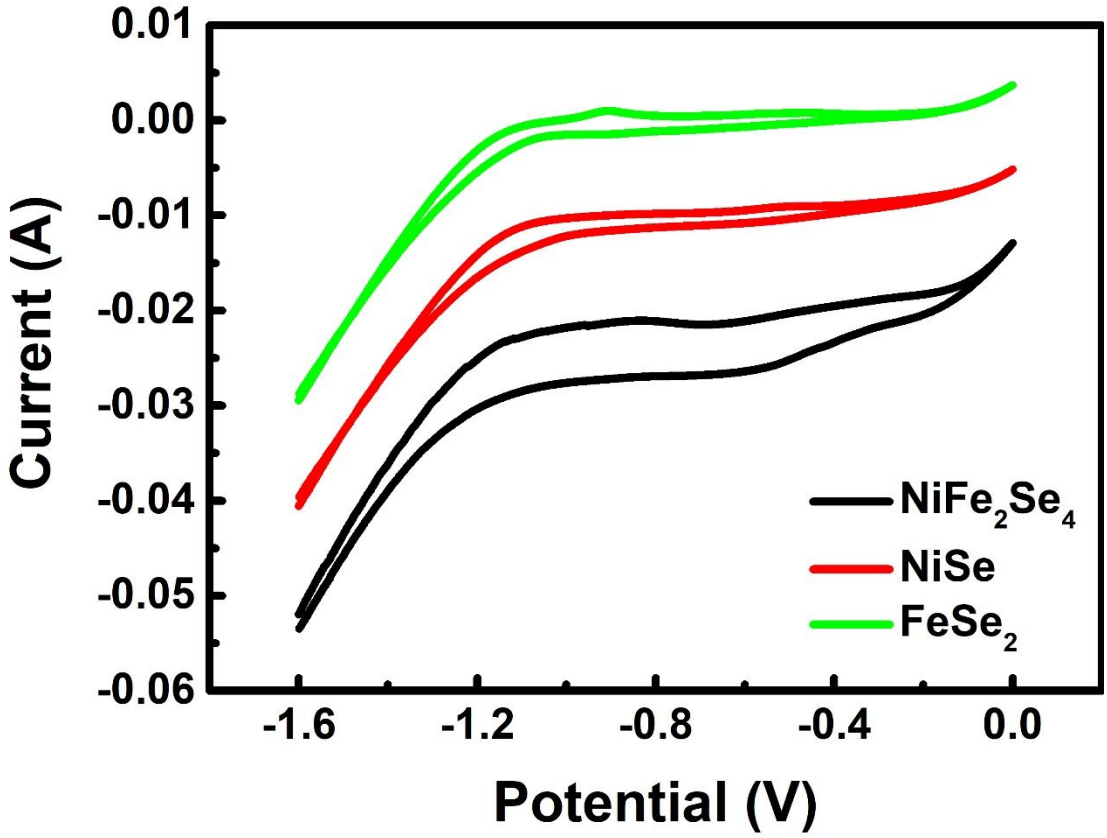

Figure S1. CV curves during electrodeposition process.

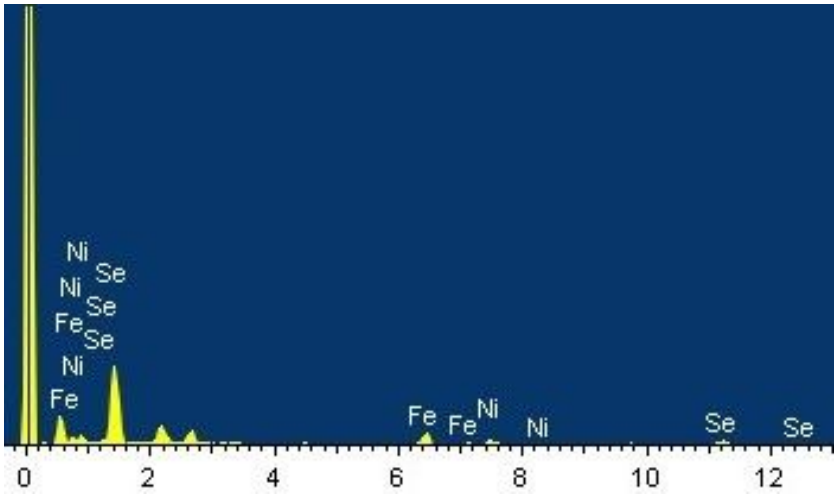

Figure S2. EDS pattern of $NiFe_2Se_4$.

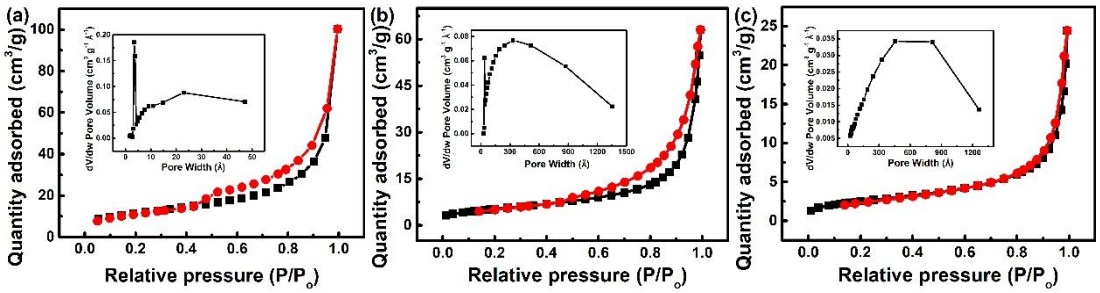

Figure S3 BET of (a) NFSe-20, (b) NiSe and (c) $FeSe_2$ samples and their corresponding BJH plot (inset).

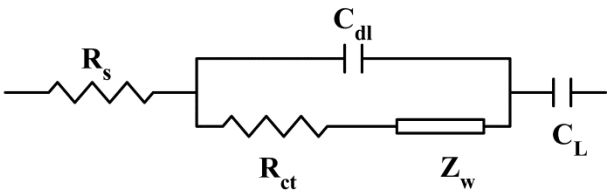

Figure S4. Equivalent circuit models used for the EIS simulation in Figure 3d and 6b.

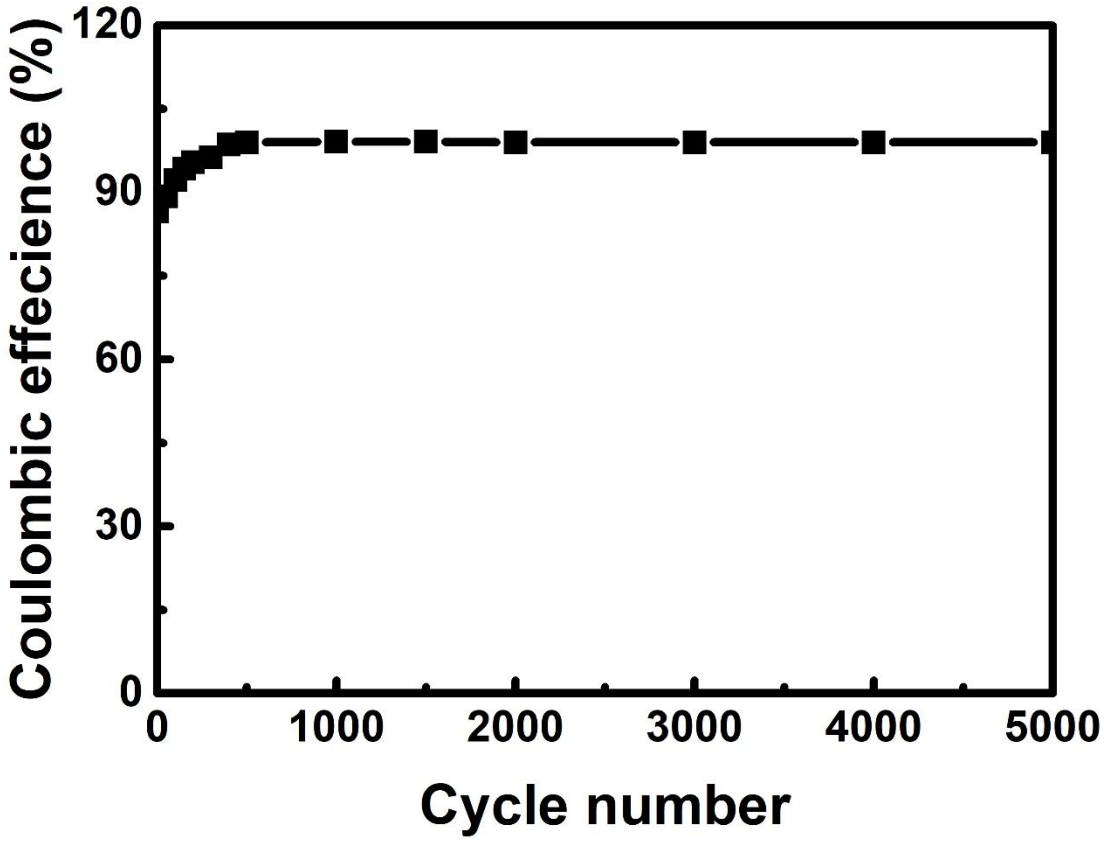

Figure S5. Coulombic efficiency at 2 A g^{-1}.

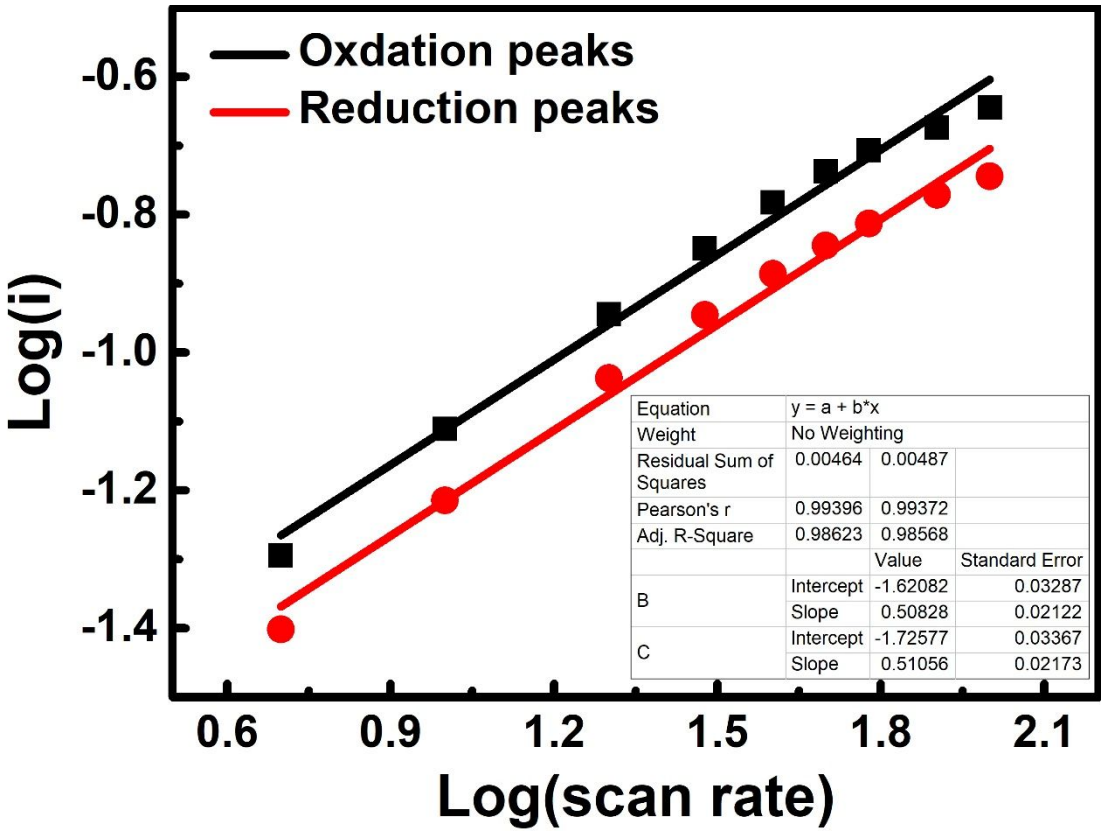

Figure S6. Power law dependence of current *i* on scan rate *v* show.

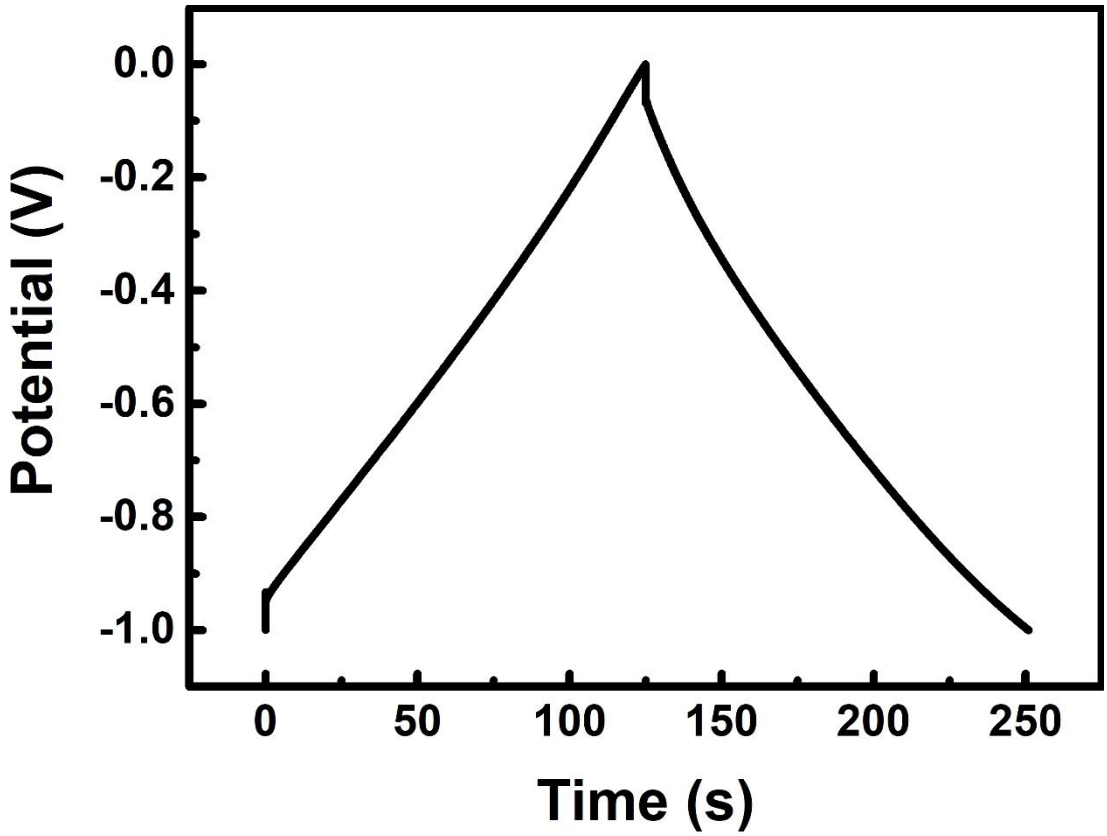

Figure S7. GCD curve of AC electrode at 2 A g^{-1}.

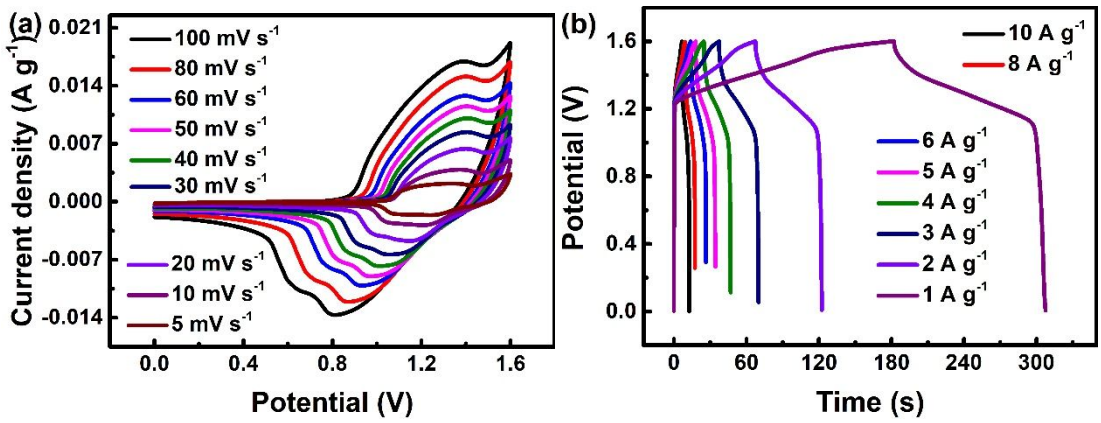

Figure S8. CV curves of NiSe//AC ASC at different scan rates, (b) GCD curves of NiSe//AC ASC at different current density.

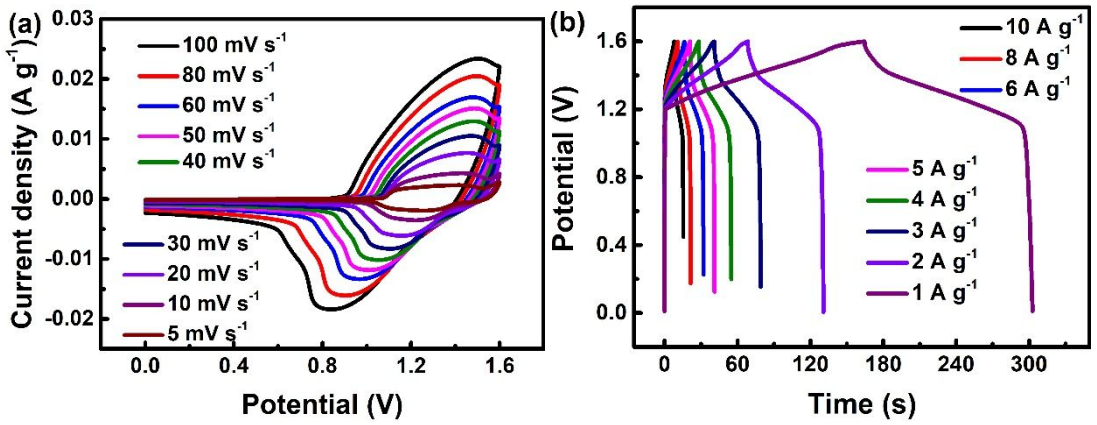

Figure S9. CV curves of $FeSe_2$//AC ASC at different scan rates, (b) GCD curves of $FeSe_2$//AC ASC at different current density.

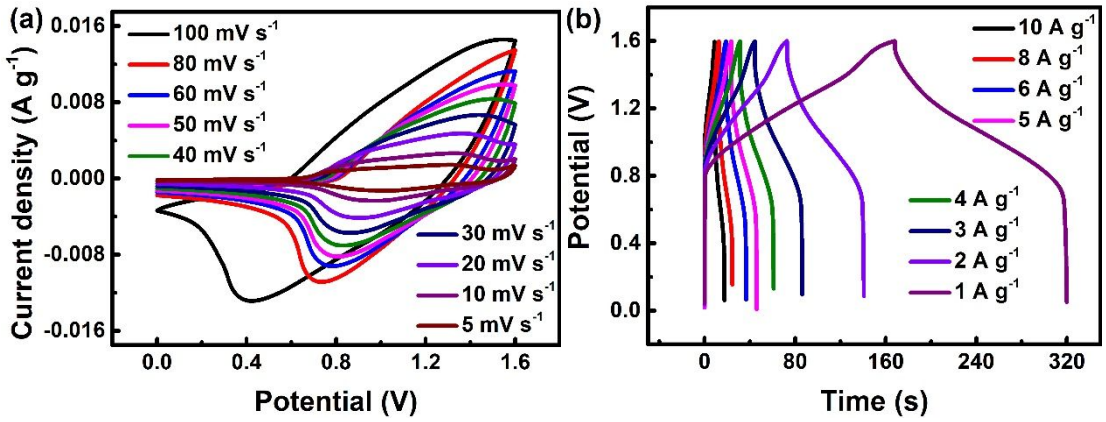

Figure S10. CV curves of NFSe-5//AC ASC at different scan rates, (b) GCD curves of NFSe-5//AC ASC at different current density.

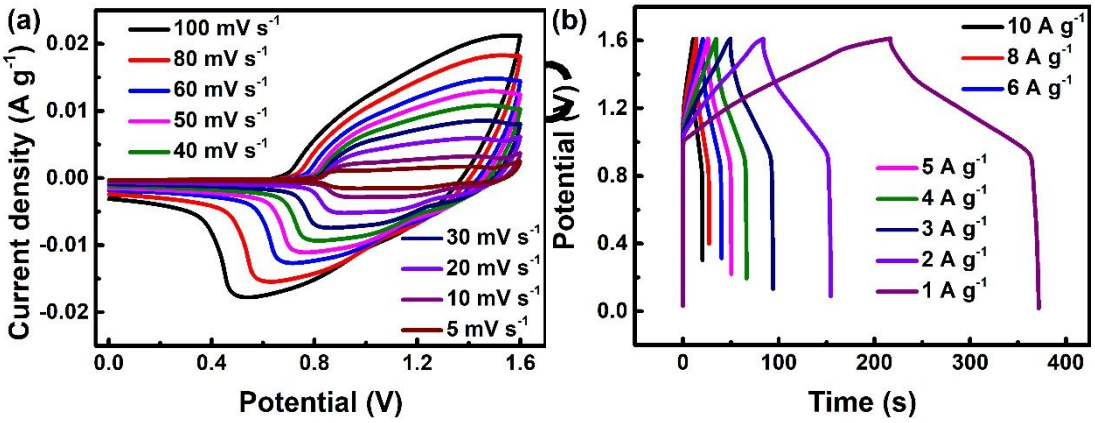

Figure S11. CV curves of NFSe-50//AC ASC at different scan rates, (b) GCD curves of NFSe-50//AC ASC at different current density.

The specific capacity (C_s, mAh g^{-1}) and specific capacitance (C_m, F g^{-1}) of the materials and ASC device was calculated from the GCD curves using eqs (S1) and eqs (S2), as follows

$$C_s = \frac{I \times \Delta t}{m \times 3.6} \quad \text{(S1)}$$

$$C_m = \frac{I \times \Delta t}{m \times \Delta V} \quad \text{(S2)}$$

where I is the discharge current density (A g^{-1}); m represents the mass of active materials grown on NF for three-electrode configurations (g); Δt is the discharge time (s); and ΔV is the potential window (V).

The energy density (E, Wh kg^{-1}) and power density (P, W kg^{-1}) of the ASCs were investigated by eqs (S3) and (S4), respectively, as follows

$$E = \frac{C_m \times \Delta V^2}{2 \times 3.6} \quad \text{(S3)}$$

$$P = \frac{3600 \times E}{\Delta t} \quad \text{(S4)}$$

In order to achieve the optimum mass ratio of as-prepared positive electrode to AC negative electrodes, we examined the charge balance using the given equation, q+ = q−. The mass of the positive electrode and negative electrode was tuned according to the following eq (S5) and (S6)

$$Q = C \times \Delta V \times m \quad \text{(S5)}$$

$$\frac{m^+}{m^-} = \frac{C_- \times \Delta V_-}{C_+ \times \Delta V_+} \quad \text{(S6)}$$

Wherein C is the specific capacity (investigated through the three-electrode configuration); + and – represents positive and negative electrodes.

Table S1 Comparison of impedance data of different electrode materials

Sample	R_s (Ω cm^2)	*CPE*, Y_o (S s^n)	Freq power. n [0<n<1]	R_{ct} (Ω m^2)	*W*, Y_o (S $s^{1/2}$ cm^{-2})
NiSe	0.65	0.0053	0.68	0.76	2.41×10^{-4}
$FeSe_2$	0.81	0.0026	0.80	0.91	1.88×10^{-17}
NFSe-5	0.62	0.0030	0.78	0.63	1.01×10^{-20}
NFSe-20	0.51	0.0046	0.73	0.51	1.19×10^{-20}
NFSe-50	0.61	0.0030	0.76	0.60	7.08×10^{-17}

Wherein, R_s is the bulk resistance of the electrochemical system, which consists of ion resistance of electrolyte, intrinsic resistance of the electrode and contact resistance between the interface of the active material and current collector. CPE is the equivalent resistance. Freq power. n represents the distribution index due to the roughness of the electrode with values ranging between 0 and 1. When n=1, it shows the pure capacitive behavior, n=0 for a pure resistance, n=0.5 represents Warburg impedance. R_{ct} is the interfacial charge transfer resistance. Z_w represents is the Warburg impedance, which is related to the electrolyte ion diffusion in the active materials.

Table S2 Comparison of electrochemical performances of some recently reported transition metal selenides-based ASCs.

Device	Electrolyte	Energy density	Reference
$NiFe_2Se_4$//AC	3M KOH	45.6 Wh kg^{-1} at 800 W kg^{-1}	This work
NiSe//AC	3M KOH	31.6 Wh kg^{-1} at 800 W kg^{-1}	This work
FeSe//AC	3M KOH	30.84 Wh kg^{-1} at 800 W kg^{-1}	This work
$(NiCo)_9Se_8$/$(NiCo)_{0.85}Se$//AC	6M KOH	37.54 Wh kg^{-1} at 842.7 W kg^{-1}	S1
$CoSe_2$@$MoSe_2$//AC	3M KOH	51.84 Wh kg^{-1} at 799.2 W kg^{-1}	S2
$Ni_{0.67}Co_{0.33}Se$//RGO	6M KOH	36.7 Wh kg^{-1} at 750 W kg^{-1}	S3
$Ni_{0.67}Co_{0.33}Se_2$//RGO	3M KOH	38.1 Wh kg^{-1} at 840 W kg^{-1}	S4
$Ni0.6Co0.4Se_2$ //BNPC	KOH/PVA gel	42.1 Wh kg^{-1}	S5
Ni@$Ni_{0.8}Co_{0.2}Se$//AC	3M KOH	17 Wh kg^{-1} at 1526.8 W kg^{-1}	S6
$Co_{0.85}Se$//AC	3M KOH	39.7 Wh kg^{-1} at 789.6 W kg^{-1}	S7
$KCo_xMn_{1-x}F_3$//AC	3M KOH	8 W hkg^{-1} at 140 W kg^{-1}	S8
Fe-Ni-Co oxide//RGO	1M KOH	40 Wh kg^{-1} at 750 W kg^{-1}	S9
$NiCo_2O_4$/$NiFe_2O_4$	6M KOH	32.4 Wh kg^{-1} at 1400 W kg^{-1}	S10
CC@CNTs@$NiSe_2$//CC@CNTs	1M KOH	11.9 $Whkg^{-1}$ at 242 W kg^{-1}	S11
CuCo2S4//NG	3M KOH	32.7Wh kg^{-1} at 794 W kg^{-1}	S12
Fe-Co-S/NF//rGO	1M KOH	43.6 Wh kg^{-1} at 770 W kg^{-1}	S13
NiCo-MOF/$Ti_3C_2T_x$//AC	2M KOH	39.5 Wh kg^{-1} at 562.5 W kg^{-1}	S14
NiCo-LDHs/rGO//rGO	3M KOH	34.5 Wh kg^{-1} at 772 W kg^{-1}	S15
NiSe-G//AC	6M KOH	50.1 Wh kg^{-1} at 816 W kg^{-1}	S16

Table S3 Fitted impedance parameters of $NiFe_2Se_4$ electrode before and after 10000 cycles.

Sample	R_s (Ω cm^2)	CPE, Y_o ($S\ s^n$)	Freq power. n [0<n<1]	R_{ct} (Ω cm^2)	W, Y_o ($S\ s^{1/2}\ cm^{-2}$)
Before cycle	0.51	0.0046	0.73	0.51	1.19×10^{-20}
After cycles	0.52	0.0027	0.69	0.73	2.88×10^{-19}

References

[S1] Liu, Y.; Yan, C.; Wang, G. G.; Li, F.; Kang, Q.; Zhang, H.; Han, J. Selenium-Rich Nickel Cobalt Bimetallic Selenide with Core-Shell Architecture Enables Superior Hybrid Energy Storage Device. Nanoscale 2020, 12, 4040–4050.

[S2] Lu, J.; Pu, L.; Wang, W.; Dai, Y. Construction of Hierarchical Cobalt-Molybdenum Selenide Hollow Nanospheres Architectures for High Performance Battery-Supercapacitor Hybrid Devices. J. Colloid Interface Sci. 2020, 563, 435–446.

[S3] Chen, H.; Chen, S.; Fan, M.; Li, C.; Chen, D.; Tian, G.; Shu, K. Bimetallic Nickel Cobalt Selenides: A New Kind of Electroactive Material for High-Power Energy Storage. J. Mater. Chem. A 2015, 3(47), 23653–23659.

[S4] Hu, Y.; Huang, C. Jiang, S.;Qin, Y.; Chen, H. C. Hierarchical Nickel-Cobalt Selenide Nanoparticles/Nanosheets as Advanced Electroactive Battery Materials for Hybrid Supercapacitors. J. Colloid Interface Sci. 2020, 558, 291–300.

[S5] Wang, Y.; Liu, R.; Sun, S.; Wu, X. Facile Synthesis of Nickel-Cobalt Selenide Nanoparticles as Battery-type Electrode for All-Solid-State Asymmetric Supercapacitors. J. Colloid Interface Sci. 2019, 549, 16–21.

[S6] Guo, K. L.; Cui, S. Z.; Hou, H. W.; Chen, W. H.; Mi, L. W. Hierarchical Ternary Ni–Co–Se Nanowires for High-Performance Supercapacitor Device Design. Dalton Trans. 2016, 45, 19458–19465.

[S7] Gong, C.; Huang, M.; Zhou, P.; Sun, Z.; Fan, L.; Lin, J.; Wu, J. Mesoporous $Co_{0.85}Se$ Nanosheets Supported on Ni Foam as a Positive Electrode Material for Asymmetric Supercapacitor. Appl. Surface Sci. 2016, 362, 469–476.

[S8] Shi, W.; Ding, R.; Li, X.; Xu, Q.; Ying, D.; Huang, Y.; Liu, E. Bimetallic Co-Mn Perovskite Fluorides as Highly-Stable Electrode Materials for Supercapacitors. Chem. - Eur. J. 2017, 23(61), 15305–15311.

[S9] Sahoo, S.; Nguyen, T. T.; Shim, J. Mesoporous Fe-Ni-Co Ternary Oxide Nanoflake Arrays on Ni Foam for High-Performance Supercapapcitor Application. J. Ind. Eng. Chem. 2018, 53, 181–190.

[S10] Duan, Y., Huo, Y., Qi, Y., Li, L., Wu, Q., Wang, C., Su. Z. Uniform $NiCo_2O_4/NiFe_2O_4$ Hollow Nanospheres with Excellent Properties for Li-ion Batteries and Supercapacitors. J. Alloys Compd., 2018, 767, 223–231.

[S11] Nie, R., Wang, Q., Sun, P., Wang, R., Yuan, Q., Wang, X. Pulsed Laser Depostion of $NiSe_2$ Film on Carbon Nanotubes for High-Performance Supercapacitor. Eng. Sci., 2019, 6, 22–29.

[S12] Dong, H., Li, Y., Chai, H., Cao, Y., Chen, X. Hydrothermal Synthesis of $CuCo_2S_4$ Nano-Structure and N-Doped Graphene for High-Performance Aqueous Asymmetric Supercapacitor. ES Energy Environ., 2019, 4, 19–16.

[S13] Le, K., Gao, M., Liu, W., Liu, J., Wang, Z., Wang, F., Murugadoss, V., Wu, S., Ding, T., Guo, Z. MOF-derived Hierarchical Core-Shell Hollow Iron-Cobalt Sulfides Nanoarrays on Ni Foam with Enhanced Electrochemical Properties for High Energy Density Asymmetric Supercapacitors. Electrochim. Acta, 2019, 323, 134826.

[S14] Wang, Y., Liu, Y. Wang, C., Liu, H., Zhang, J., Liu, J., Fan, J., Ding, T. Ryu, J. E., Guo, Z. Significantly Enhanced Ultrathin NiCo-based MOF Nanosheet Electrodes Hybrided with $Ti_3C_2T_x$ Mxene for High Performance Asymmetric Supercapacitor. Eng. Sci., 2020, 9, 50–59.

[S15] Le, K., Wang, Z., Wang, F., Wang, Q., Shao, Q., Murugadoss, V., Wu, S., Liu, W., Liu, J., Gao, Q., Guo, Z. Sandwich-like NiCo Layered Double Hydroxide/Reduced Graphene Oxide Nanocomposite Cathodes for High Energy Density Asymmetric Supercapacitors. Dalton Trans., 2019, 48, 5193.

[S16] Kirubasankar, B., Murugadoss, V., Lin, J., Ding, T., Dong, M., Liu, H., Zhang, J., Li, T., Wang, N., Guo, Z., Angaiah, S. In Situ Grown Nickel Selenide on Graphene Nanohybrid Electrodes for High Energy Density Asymmetric Supercapacitors. Nanoscale, 2018, 10, 20414.